LETTERS

The subcellular organization of neocortical excitatory connections

Leopoldo Petreanu[1], Tianyi Mao[1], Scott M. Sternson[1] & Karel Svoboda[1]

Understanding cortical circuits will require mapping the connections between specific populations of neurons[1], as well as determining the dendritic locations where the synapses occur[2]. The dendrites of individual cortical neurons overlap with numerous types of local and long-range excitatory axons, but axodendritic overlap is not always a good predictor of actual connection strength[3–5]. Here we developed an efficient channelrhodopsin-2 (ChR2)-assisted method[6–8] to map the spatial distribution of synaptic inputs, defined by presynaptic ChR2 expression, within the dendritic arborizations of recorded neurons. We expressed ChR2 in two thalamic nuclei, the whisker motor cortex and local excitatory neurons and mapped their synapses with pyramidal neurons in layers 3, 5A and 5B (L3, L5A and L5B) in the mouse barrel cortex. Within the dendritic arborizations of L3 cells, individual inputs impinged onto distinct single domains. These domains were arrayed in an orderly, monotonic pattern along the apical axis: axons from more central origins targeted progressively higher regions of the apical dendrites. In L5 arborizations, different inputs targeted separate basal and apical domains. Input to L3 and L5 dendrites in L1 was related to whisker movement and position, suggesting that these signals have a role in controlling the gain of their target neurons[9]. Our experiments reveal high specificity in the subcellular organization of excitatory circuits.

We recorded from pyramidal neurons in neocortical brain slices containing ChR2- expressing axons[7] (Fig. 1a). To map the dendritic locations of input from ChR2-positive axons (Supplementary Fig. 1), we used a laser to depolarize these axons only in the vicinity of the laser beam (that is, with action potentials blocked), triggering local glutamate release (subcellular ChR2-assisted circuit mapping (sCRACM)). We blocked Na$^+$ channels (1 μM tetrodotoxin (TTX)) and the K$^+$ channels that are critical for repolarization of the axon (200 nM α-dendrotoxin or 100 μM 4-aminopyridine (4-AP)) (Fig. 1b)[10]. Under these conditions, photostimulation with short (1-ms) light pulses (<2 mW) triggered robust excitatory postsynaptic currents (EPSC$_{sCRACM}$; Fig. 1b). Higher light intensities caused larger EPSC$_{sCRACM}$ amplitudes (Fig. 1c) and shorter onsets (Supplementary Fig. 2). As the cylindrical laser beam was scanned over the dendrites of a recorded neuron (map pattern: 12 × 24 grid, 50-μm spacing), EPSC$_{sCRACM}$ were detected only when the laser beam overlapped with the dendritic arborization of the recorded cell and with ChR2-positive axons (Fig. 1b, d–f), indicating that under these conditions light depolarizes ChR2-positive axons to cause local release of neurotransmitter. Converting EPSC$_{sCRACM}$ into pixel values
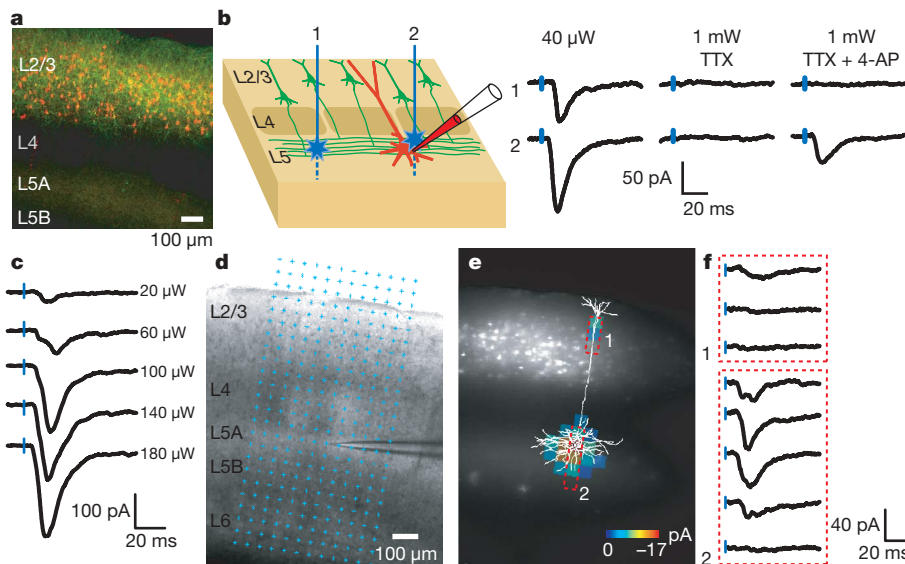

Figure 1 | Subcellular ChR2-assisted circuit mapping. a, Confocal image showing L2/3 neurons expressing mCherry (red) and ChR2-Venus (green) in the barrel cortex. **b**, Left: sketch of the photostimulation geometry. Right: excitatory postsynaptic currents evoked by photostimuli corresponding to the locations indicated in the sketch. Blue tickmarks indicate the laser pulse. Laser power is indicated at top. **c**, EPSC$_{sCRACM}$ evoked by photostimulation with increasing laser powers (right). **d**, Bright-field image of a brain slice showing the recording pipette and the photostimulation grid (blue dots). **e**, sCRACM map overlaid on a fluorescence image, showing ChR2-positive neurons, and the reconstructed dendrite of the recorded neuron (same experiment as **d**). Non-zero EPSC$_{sCRACM}$ are colour-coded to represent mean amplitude. **f**, EPSC$_{sCRACM}$ recorded in the boxed regions in **e**.

[1]Janelia Farm Research Campus, Howard Hughes Medical Institute, Ashburn, Virginia 20147, USA.

(EPSC$_{sCRACM}$ averaged over a time window 0–75 ms post-stimulus) provides a two-dimensional 'image' of the distribution of specific input within the dendritic arborizations of the recorded cell (Fig. 1e, f). Measurements of the point spread function revealed that sCRACM maps specific types of input with ~60-μm spatial resolution (Supplementary Fig. 3).

EPSC$_{sCRACM}$ amplitudes depend on the density of ChR2-positive axons, the fraction of axons that make synapses with the recorded neuron, the strength of the synapses and their electrotonic distances from the soma[11] (see Methods). Because the density of ChR2-positive axons varies between preparations, sCRACM maps were normalized to the largest pixels within a map and thus represent the relative strengths of input within the dendritic tree. Repeated sCRACM maps were reproducible at the level of single pixels (Supplementary Fig. 4), and the structure of peak-normalized maps was similar across a large range of light intensities (Supplementary Fig. 4).

Multiple types of axon overlap with the dendrites of cortical neurons[5,12–17]. Some axons arise locally[5,14,18], whereas others ascend from the thalamus[15,16] or descend from higher cortical areas[17]. To determine which axons in a target region connect with a particular cell type, and the spatial distributions of specific inputs within the dendritic tree, we expressed ChR2 in five distinct axonal populations (in separate experiments) that overlap with pyramidal cell dendrites in the barrel cortex (Supplementary Fig. 5).

The spatial distribution of labelled axons in the barrel cortex was largely in agreement with previous anatomical studies (Supplementary Fig. 5). Projections from the ventral posterior medial nucleus (VPM) of the thalamus were focused in L4 and at the border of L5 with L6 (Fig. 2a, Supplementary Fig. 5)[16], but diffuse axons were found throughout all cortical layers[15]. L4 axons arborized in L4 and ascended into L2/3, up to the lower edge of L1 (ref. 18); a weaker projection descended into L5 and L6 (ref. 18). Axons from L2/3 pyramidal cells arborized within L2/3 and on the border of L5A with

L5B (refs 7, 14). Axons from the primary whisker motor cortex (M1) arborized densely in L1, and more diffusely in L5 and L6 (ref. 17). A dense bundle of ascending M1 axons was often apparent next to the most medial barrels (Fig. 2a, arrowhead). Axons from the posterior medial nucleus (POm) of the thalamus were focused in L5A, and more weakly in L1 (ref. 15).

We mapped specific types of input within the dendritic trees of individual L3 cells (Fig. 2a). Maps were then averaged across cells either aligned on the pia (Fig. 2b), to visualize the laminar location of the inputs, or aligned on the soma, to measure the location of the inputs relative to the soma (Fig. 2c). L3 cells received input from all five projections. Each input overlapped with a single contiguous dendritic subregion (Fig. 2c, d). Ascending input from VPM to L3 (VPM → L3) was focused on the bottom part of the basal dendritic arborizations. Input from ascending L4 → L3 axons was centred on the soma and basal arborization, above the input from VPM. Input from recurrent L2/3 → L3 axons was mostly in the upper basal dendrites and the apical oblique dendrites, above the input from L4 (see also Supplementary Fig. 6). Feedback from M1 targeted the tuft branches in L1, above the input from L2/3. The positions of VPM, L4, L2/3 and M1 input along the apical axis of L3 neurons mirrors the flow of excitation within the cortical circuit: more peripheral input impinges on lower parts of the dendritic arborization, whereas more central input impinges on higher parts of the dendritic arborization. During somatosensation, L3 neurons thus receive an ascending wave of excitatory input. POm → L3 input was weighted towards L1, although it was distributed relatively broadly, spanning most of the dendritic arborization.

We next mapped the same group of five inputs within the dendrites of L5 pyramidal neurons. Both L5A and L5B pyramidal cells received input from L4, L2/3, M1 and VPM (Fig. 3a, b, Supplementary Fig. 7). To quantify the strength of input from defined axonal projections across postsynaptic cells in different layers, we recorded from pairs
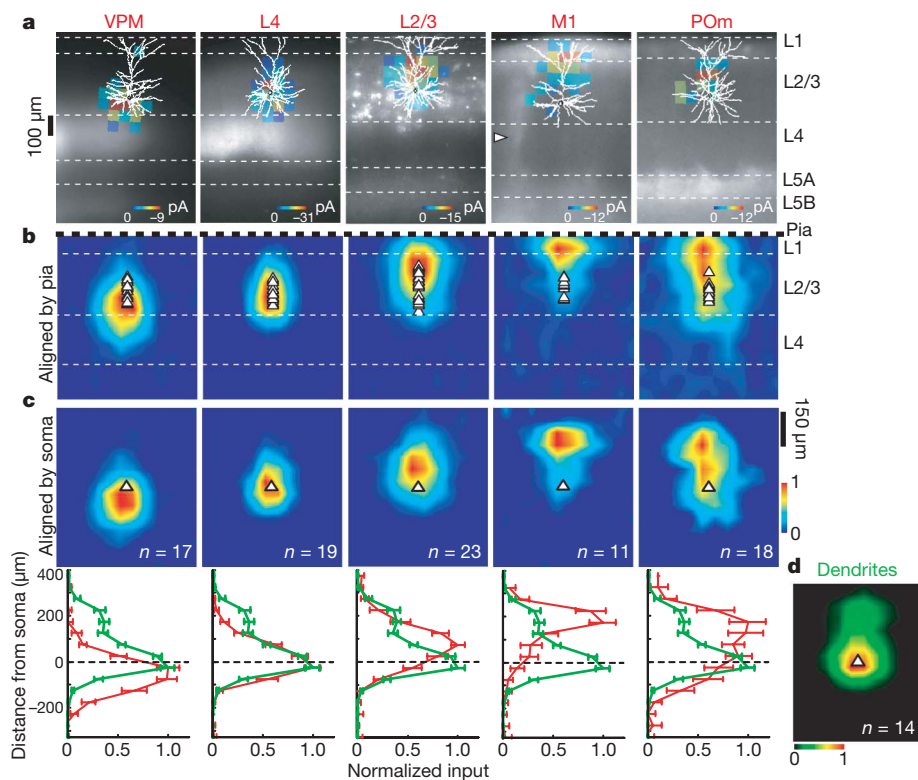

Figure 2 | Subcellular distribution of inputs onto L3 pyramidal neurons. a, Examples of sCRACM maps overlaid on reconstructed dendrites and fluorescence images showing ChR2-positive axons (VPM, M1 and POm) or axons and dendrites (L2/3 and L4). White arrowhead, bundle of ascending axons from M1. **b**, Group averages aligned by pia position (white triangles, soma position). **c**, Top: group averages aligned by soma position; bottom: vertical profiles of the distribution of synaptic input (red) and the dendritic length density (green; from **d**). Error bars, s.e.m. **d**, Average normalized dendritic length density of L3 pyramidal neurons.
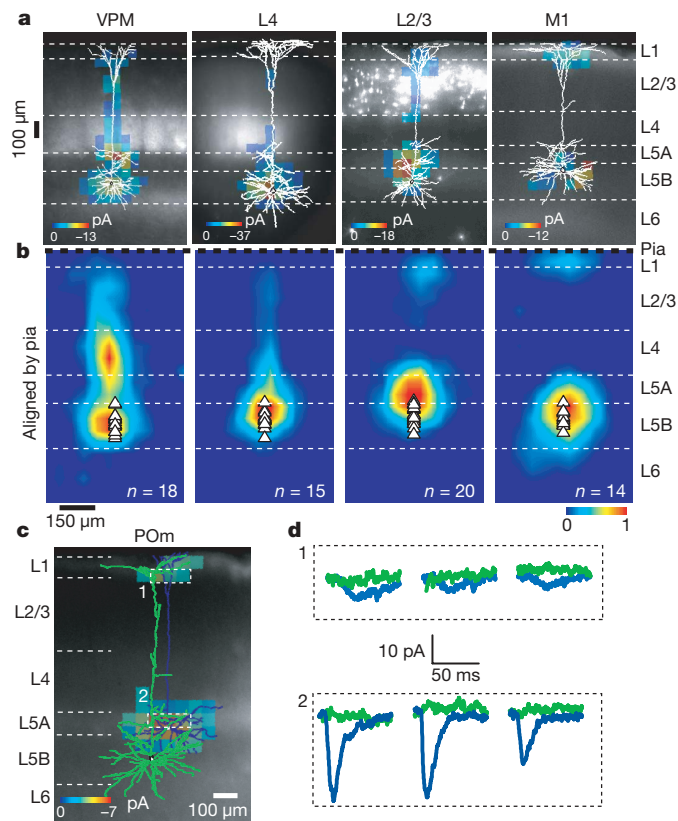
Figure 3 | Subcellular distribution of inputs onto L5B pyramidal neurons.
a, Examples of sCRACM maps overlaid on reconstructed dendritic
arborizations and fluorescence images. **b**, Group averages aligned by pia
position (white triangles, soma position). **c**, sCRACM map of POm input
onto a L5A pyramidal cell (blue). No responses were detected on the L5B
neuron (green). **d**, EPSC$_{sCRACM}$ recorded on the L5A neuron (blue) or the
L5B neuron (green) when photostimulating the boxed regions in **c**. The
stimulus occurred at the beginning of each trace.

of cells in the same column with identical laser powers (Supplementary
Table 1). L5B cells received 62-fold less input from POm in comparison
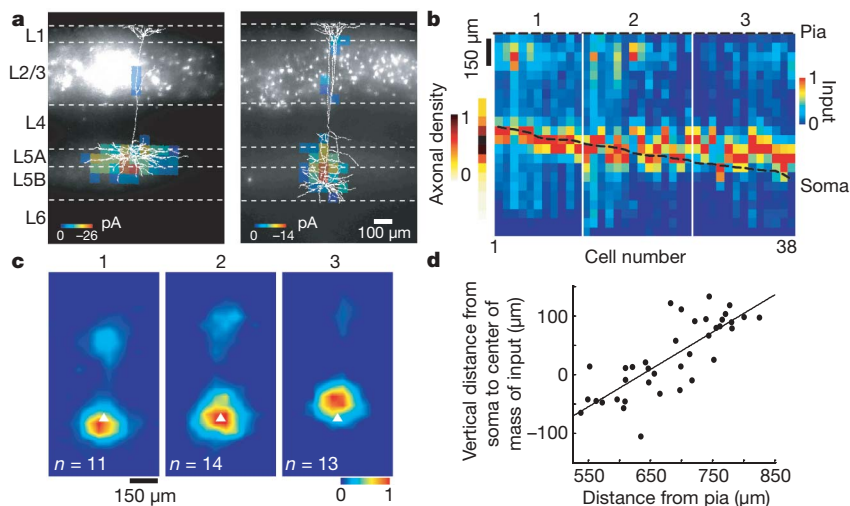with L5A cells, despite there being pronounced overlap between L5B

dendrites and POm axons (dendritic length: L5A pyramidal cells
($n = 12$) in L1, 871 ± 546 μm, in L5A, 2,158 ± 899 μm; L5B pyramidal
cells ($n = 13$) in L1, 1,609 ± 732 μm, in L5A, 761 ± 350 μm; see Fig. 3c,
d, Supplementary Fig. 7 and Supplementary Table 1). L5A, but not
L5B, pyramidal cells received significant input from POm. This con-
firms that average cortical connectivity between populations of neu-
rons cannot always be deduced from the structure of axons and
dendrites alone[3–5]. Because L5B pyramidal neurons constitute the main
projection from barrel cortex to POm[19], there appears to be no dis-
ynaptic loop between these two areas.

By contrast with L3 cells, the inputs on L5 cells were not limited to a
single compartment, but were split into basal and apical domains
(Fig. 3, Supplementary Fig. 7), reinforcing the view that large pyr-
amidal neurons consist of multiple, weakly coupled compartments[20].
Here we describe the inputs to L5B neurons (Fig. 3), and then highlight
the differences with L5A neurons (Supplementary Fig. 7). VPM → L5B
input was distributed along most of the dendritic arborization, but was
most prominent on the basal dendrites and in L4. L4 → L5B input was
centred on the basal dendrites, overlapping with VPM input; weak
input was also detected along the apical dendrite up to the edge of
L1. L2/3 → L5B input was focused on the upper basal and apical
oblique dendrites, as well as on the apical tuft in L2. M1 → L5B input
was on the basal dendrites and on the apical tuft in L1.

Inputs to L5A pyramidal neurons similarly targeted dual dendritic
compartments (Supplementary Fig. 7), with some differences.
POm → L5A input was prominent, both on the basal dendrites and
the apical tuft in L1. Unlike for L2/3 → L5B input, L2/3 → L5A input
was centred on the basal dendrites (Fig. 4a, Supplementary Fig. 7).
For all L5 neurons taken together, there was a monotonic relation-
ship between the laminar position of the recorded cell and the loca-
tion of L2/3 input relative to the soma position (Fig. 4b–d). The
axodendritic overlap of L2/3 axons and L5 dendrites is most likely
an important factor in determining the subcellular location of L2/
3 → L5 input.

sCRACM maps functional neural circuits with subcellular resolu-
tion. Because sCRACM maps are based on somatic measurements of
synaptic currents generated in the dendrites, signal attenuation due
to dendritic filtering influences the structure of the maps. For
example, input on the apical tufts of L5 neurons could be reduced
several-fold relative to more proximal input[11]. sCRACM maps thus
represent a 'somatocentric' view of the dendritic distribution of

**Figure 4 | The laminar position of L5 pyramidal neurons determines the
dendritic location of L2/3 inputs. a**, Examples of the subcellular
distribution of L2/3 input onto superficial (L5A, left) or deep (L5B, right)
pyramidal neurons. **b**, Vertical profiles of the subcellular distribution of L2/
3 → L5 inputs. Each column represents one cell, ordered by cortical depth.
Cells were aligned by pia position. The relative density of L2/3 axons in the
deep layers is indicated to the left of the panel. **c**, Average subcellular location

of L2/3 input (aligned by soma position) of L5 cells grouped by increasing
distance from the pia (groups correspond to the white lines in **b**; white
triangles, soma position). **d**, Plot of the vertical distance from the soma to the
centre of mass of L2/3 input on the perisomatic region (<285 μm from the
soma) of L5 pyramidal neurons versus cortical depth. The line is a regression
fit.

synaptic input, where electrotonically distant synapses will appear relatively weak (Supplementary Fig. 8).

We mapped input from VPM, L4, L2/3, M1 and POm, within the dendritic arborizations of L3 and L5 neocortical pyramidal cells. L3 and L5 cells received input from most axonal populations, with the exception of POm→L5B. Some connections (VPM→L3, VPM→L5A, VPM→L5B, POm→L5A, L4→L3, L4→L5A, L2/3→L3, L2/3→L5A and L2/3→L5B) have been previously characterized[3,14,18,21,22], whereas others (M1→L3, M1→L5A, M1→L5B, POm→L3 and L4→L5B,) were previously unknown.

We identified several connections in L1: M1→L3, M1→L5A, M1→L5B, POm→L3 and POm→L5A. Axons from VPM, L2/3 and L4 did not contribute significantly to L1 input. POm neurons are thought to encode aspects of whisker position[23] and whisker M1 carries signals related to voluntary whisker control[24]. Our findings suggest that synapses in L1 carry signals related to whisker movement and position.

The spatial segregation of specific types of input within dendritic arborizations might subserve several functions. Segregated inputs are less likely to interact at the level of synaptic plasticity[25]. Spatially clustered co-active synapses are more efficacious in driving post-synaptic neurons than spatially distributed synapses[26,27]. For a fixed number of synapses, spatial segregation of different axonal populations within dendritic arborizations might thus strengthen the effective coupling between pre- and postsynaptic populations.

METHODS SUMMARY

Specific neuronal populations were labelled with ChR2 *in vivo* either by *in utero* electroporation[7,28] (L2/3 pyramidal cells), adeno-associated-virus infection (VPM, POm, M1) or infection with a Cre-recombinase-dependent adeno-associated virus[29] in mice expressing Cre (L4)[30]. Acute coronal slices were prepared from young adult (postnatal day 26–34) mice. Pyramidal neurons in L3 and L5 were recorded in a voltage clamp at room temperature (22–24 °C). Photostimulation was with blue (473-nm) laser pulses (duration, 1 ms; inter-stimulus interval, 400 ms; beam diameter, 6–16 μm) in the presence of TTX (1 μM), 3-((R)-2-carboxypiperazin-4-yl)-propyl-1-phosphonic acid (CPP, 5 μM) and 4-AP (100 μM).

Full Methods and any associated references are available in the online version of the paper at www.nature.com/nature.

1. Douglas, R. J. & Martin, K. A. Mapping the matrix: the ways of neocortex. *Neuron* **56**, 226–238 (2007).
2. London, M. & Hausser, M. Dendritic computation. *Annu. Rev. Neurosci.* **28**, 503–532 (2005).
3. White, E. L. Specificity of cortical synaptic connectivity: emphasis on perspectives gained from quantitative electron microscopy. *J. Neurocytol.* **31**, 195–202 (2002).
4. Dantzker, J. L. & Callaway, E. M. Laminar sources of synaptic input to cortical inhibitory interneurons and pyramidal neurons. *Nature Neurosci.* **3**, 701–707 (2000).
5. Shepherd, G. M. G., Stepanyants, A., Bureau, I., Chklovskii, D. B. & Svoboda, K. Geometric and functional organization of cortical circuits. *Nature Neurosci.* **8**, 782–790 (2005).
6. Nagel, G. *et al.* Channelrhodopsin-2, a directly light-gated cation-selective membrane channel. *Proc. Natl Acad. Sci. USA* **100**, 13940–13945 (2003).
7. Petreanu, L., Huber, D., Sobczyk, A. & Svoboda, K. Channelrhodopsin-2-assisted circuit mapping of long-range callosal projections. *Nature Neurosci.* **10**, 663–668 (2007).
8. Zhang, F., Wang, L. P., Boyden, E. S. & Deisseroth, K. Channelrhodopsin-2 and optical control of excitable cells. *Nature Methods* **3**, 785–792 (2006).
9. Larkum, M. E., Senn, W. & Luscher, H. R. Top-down dendritic input increases the gain of layer 5 pyramidal neurons. *Cereb. Cortex* **14**, 1059–1070 (2004).
10. Shu, Y., Yu, Y., Yang, J. & McCormick, D. A. Selective control of cortical axonal spikes by a slowly inactivating K+ current. *Proc. Natl Acad. Sci. USA* **104**, 11453–11458 (2007).
11. Williams, S. R. & Mitchell, S. J. Direct measurement of somatic voltage clamp errors in central neurons. *Nature Neurosci.* **11**, 790–798 (2008).
12. Binzegger, T., Douglas, R. J. & Martin, K. A. A quantitative map of the circuit of cat primary visual cortex. *J. Neurosci.* **24**, 8441–8453 (2004).
13. Gilbert, C. D. Microcircuitry of the visual cortex. *Annu. Rev. Neurosci.* **6**, 217–247 (1983).
14. Feldmeyer, D., Lubke, J. & Sakmann, B. Efficacy and connectivity of intracolumnar pairs of layer 2/3 pyramidal cells in the barrel cortex of juvenile rats. *J. Physiol. (Lond.)* **575**, 583–602 (2006).
15. Lu, S. M. & Lin, R. C. S. Thalamic afferents of the rat barrel cortex: a light- and electron-microscopic study using *Phaseolus vulgaris* leucoagglutinin as an anterograde tracer. *Somatosens. Mot. Res.* **10**, 1–16 (1993).
16. Koralek, K. A., Jensen, K. F. & Killackey, H. P. Evidence for two complementary patterns of thalamic input to the rat somatosensory cortex. *Brain Res.* **463**, 346–351 (1988).
17. Veinante, P. & Deschenes, M. Single-cell study of motor cortex projections to the barrel field in rats. *J. Comp. Neurol.* **464**, 98–103 (2003).
18. Lubke, J., Roth, A., Feldmeyer, D. & Sakmann, B. Morphometric analysis of the columnar innervation domain of neurons connecting layer 4 and layer 2/3 of juvenile rat barrel cortex. *Cereb. Cortex* **13**, 1051–1063 (2003).
19. Hoogland, P. V., Welker, E. & Van der Loos, H. Organization of the projections from barrel cortex to thalamus in mice studied with Phaseolus vulgaris-leucoagglutinin and HRP. *Exp. Brain Res.* **68**, 73–87 (1987).
20. Mainen, Z. F. & Sejnowski, T. J. Influence of dendritic structure on firing pattern in model neocortical neurons. *Nature* **382**, 363–366 (1996).
21. Bureau, I., von Saint Paul, F. & Svoboda, K. Interdigitated paralemniscal and lemniscal pathways in the mouse barrel cortex. *PLoS Biol.* **4**, e382 (2006).
22. Thomson, A. M. & Bannister, A. P. Interlaminar connections in the neocortex. *Cereb. Cortex* **13**, 5–14 (2003).
23. Yu, C., Derdikman, D., Haidarliu, S. & Ahissar, E. Parallel thalamic pathways for whisking and touch signals in the rat. *PLoS Biol.* **4**, e124 (2006).
24. Berg, R. W. & Kleinfeld, D. Vibrissa movement elicited by rhythmic electrical microstimulation to motor cortex in the aroused rat mimics exploratory whisking. *J. Neurophysiol.* **90**, 2950–2963 (2003).
25. Harvey, C. D. & Svoboda, K. Locally dynamic synaptic learning rules in pyramidal neuron dendrites. *Nature* **450**, 1195–1200 (2007).
26. Polsky, A., Mel, B. W. & Schiller, J. Computational subunits in thin dendrites of pyramidal cells. *Nature Neurosci.* **7**, 621–627 (2004).
27. Losonczy, A. & Magee, J. C. Integrative properties of radial oblique dendrites in hippocampal CA1 pyramidal neurons. *Neuron* **50**, 291–307 (2006).
28. Saito, T. & Nakatsuji, N. Efficient gene transfer into the embryonic mouse brain using *in vivo* electroporation. *Dev. Biol.* **240**, 237–246 (2001).
29. Atasoy, D., Aponte, Y., Su, H. H. & Sternson, S. M. A FLEX switch targets Channelrhodopsin-2 to multiple cell types for imaging and long-range circuit mapping. *J. Neurosci.* **28**, 7025–7030 (2008).
30. Liao, G. Y. & Xu, B. Cre recombinase-mediated gene deletion in layer 4 of murine sensory cortical areas. *Genesis* **46**, 289–293 (2008).

Author Contributions L.P. and K.S. designed the experiments. L.P. performed the experiments with help from T.M. (viral injections in M1 and related recordings). S.S. provided critical reagents. L.P. and K.S. analysed the data and wrote the paper.

Author Information Reprints and permissions information is available at www.nature.com/reprints. Correspondence and requests for materials should be addressed to K.S. (svobodak@janelia.hhmi.org).

METHODS

Electrophysiology and photostimulation. Neurons were patched with borosilicate pipettes (resistance, 4–6 MΩ). The intracellular solution contained 128 mM K-gluconate, 4 mM MgCl$_2$, 10 mM HEPES, 1 mM EGTA, 4 mM Na$_2$ATP, 0.4 mM Na$_2$GTP, 10 mM sodium phosphocreatine, 3 mM sodium L-ascorbate and 0.015 mM Alexa-594 (Molecular Probes) (pH 7.25, 290 mosM). Cells were recorded at depths of 50 to 95 μm in the brain slice. Data were acquired using custom programs (Ephus, available at https://openwiki.janelia.org/). Photostimulation was with a blue laser (473 nm; Crystal Laser). The beam's position was controlled with galvanometers (6210H, Cambridge Scanning). The beam was delivered through an air immersion objective (×4, 0.16 numerical aperture; UPlanApo, Olympus). The optics were designed to generate a nearly cylindrical beam (~6–16 μm, full-width at half-maximum at the focal plane). The duration and intensity of the light pulses were controlled with a Pockels cell (ConOptics) and a shutter (LS3, Uniblitz).

For sCRACM mapping, we delivered light pulses (duration, 1 ms; inter-stimulus interval, 400 ms) on a 12 × 24 grid with 50-μm spacing (Fig. 1d). The grid area (0.6 × 1.2 mm^2) included the entire thickness of the cortical grey matter. Stimuli were given in a spatial sequence pattern designed to maximize the time between stimuli to neighbouring spots[31]. To avoid sequence-specific responses during consecutive mapping, we flipped and rotated the stimulus pattern between maps. TTX (1 μM), CPP (5 μM) and 4-AP (100 μM) were added to the bath. Without 4-AP (or α-dendrotoxin (200 nM); Alomone Labs), TTX (1 μM) abolished 98 ± 1.9% of the excitatory postsynaptic currents evoked in the absence of drugs (six cells, 573 sites), even at high light intensities (>1 mW; Fig. 1b). When mapping inputs from L4 axons, we also added bicuculline (10 μM) to block contributions from GABAergic neurons in L4 (ref. 30). EPSC$_{sCRACM}$ were recorded in voltage clamp (−75 mV). Access resistances were <40 MΩ and stable (<20% change during the experiment); resting potentials were less than −55 mV.

EPSC$_{sCRACM}$ have relatively long delays (mean, 10.4 ± 2.5 ms; L2/3 → L5A perisomatic responses; <110 μm from the soma; 146 sites; 18 cells; Supplementary Fig. 2), most likely reflecting the slow charging and discharging of the axonal membrane (Supplementary Fig. 9). The delays varied across photostimulation sites (range, 6.4–21 ms) and EPSC$_{sCRACM}$ rise times (mean (10–90%), 6.5 ± 3.1 ms; range, 2.4–18.3 ms) and decay times (mean, 35 ± 28 ms; range, 6.2–160 ms) were long. EPSC$_{sCRACM}$ on occasion displayed multiple peaks. Minimal stimulation experiments (Supplementary Fig. 2c) revealed that unitary currents were slightly desynchronized at a single photostimulation location (latency jitter, 1.03 ± 0.5 ms; $n = 6$) and highly desynchronized across different locations (latency range, 10.4–17.2 ms; mean, 15.2 ± 3 ms; $n = 6$; Supplementary Fig. 2). The temporal smearing of the EPSC$_{sCRACM}$ waveform is therefore dominated by differences in latencies across different synapses. The rise time of the responses increased with distance to the soma, along both the apical and basal dendrites, consistent with filtering expected from cable theory (Supplementary Fig. 2)[32,33].

For each recorded cell, laser powers were adjusted to cause EPSC$_{sCRACM}$ with peak amplitudes of approximately −75 pA (L2/3 pyramidal neurons, −72 ± 47 pA; L5 pyramidal neurons, −84 ± 45 pA). The corresponding laser powers varied over one order of magnitude (120 μW–1.9 mW at the specimen plane), reflecting variations in the fraction of ChR2-positive axons and ChR2 expression levels across mice. sCRACM maps were repeated 2–5 times for each cell (Supplementary Fig. 4). After the recordings, dendritic arborizations were imaged using fluorescence microscopy (Retiga 2000RV, QImaging) and subsequently processed for biocytin staining and reconstructed. Only data from neurons where the apical dendrites ran parallel to the slice surface were included in the analysis.

Because photostimulation was with a cylindrical beam, sCRACM maps represent the two-dimensional projections of the three-dimensional distribution of inputs. As a consequence, the peak values of the distribution of inputs were sometimes centred on the somata, although somata are mostly devoid of excitatory synapses (Figs 2 and 3). This is analogous to the two-dimensional projection of the density of basal dendrites, which also peaks on the soma (Figs 2 and 3, Supplementary Fig. 7). Furthermore, under our conditions the sCRACM resolution was ~60 μm, which is large in comparison with the diameters of most somata.

Data analysis. Individual pixels of sCRACM maps at position (x, y) ($Q(x, y)$) were computed as the mean EPSC$_{sCRACM}$ amplitude in a response window from 0 to 75 ms after the stimulus, and thus are a measure of charge. For consistency with previous studies, and because synaptic current is a more familiar unit, data are given in units of picoamperes. Q is given by

$$Q(x,y) \approx \rho_a(x,y)\rho_b(x,y)fqg(L(x,y))$$

where ρ_a and ρ_b are the densities of axons and dendrites, respectively; f is the filling fraction, defined as the fraction of axons making synapses with nearby dendrites[34]; q is the charge per synapse per light flash; and $g(L)$ is the dendritic attenuation as a function of electrotonic distance, $L(x, y)$, between the site of photostimulation and the soma. Because of dendritic attenuation, Q provides a somatocentric view of the synaptic input (see Supplementary Discussion). Because ρ_a, and possibly q, depends on details of the gene transfer method, it is challenging to compare the strengths of different projections onto the same cell. As ρ_a varies between preparations, sCRACM maps were normalized to the largest pixels within a map, and thus represent the relative strength of input within the dendritic tree.

Averaged EPSC$_{sCRACM}$ were scored as non-zero if their amplitudes (0–50 ms post-stimulus) were more than five times larger than the standard deviation of the baseline (Figs 1e, 2a, 3a and 4a, Supplementary Figs 3 and 7). Maps were either aligned on the soma or on the pia. In the case of alignment on the pia, it was necessary to correct for variations in cortical thickness; individual maps were therefore morphed by linear interpolation to a template based on the average cortical thickness. Similarly, the cortical depth of individual neurons (Fig. 4) was also normalized to the average depth across slices. Individual maps are presented as raw pixel images, whereas group averages are linearly interpolated without smoothing (for display only). To measure the density of L2/3 axons (Fig. 4b), we measured and peak-normalized mCherry fluorescence along the cortical axis in L4 to L6 in *in utero* electroporated animals ($n = 5$).

sCRACM resolution. The effective resolution of sCRACM mapping can be inferred from the point spread function. We measured the point spread function from the spatial distribution of the photostimulation sites that produce detectable responses in the vicinity of isolated dendritic branches. L5A cells often received input from L2/3 neurons along a single unbranched apical dendrite within L2/3 (Supplementary Fig. 3). To measure sCRACM resolution, we first identified the peak of L2/3 input on the apical dendrites of L5A cells within L2/3. We next photostimulated in a line across the apical dendrite, through the peak of L2/3 input (12 positions, 15-μm spacing between stimuli, inter-stimulus interval of 6 s; Supplementary Fig. 3a). Because the activated synapses were on a single dendritic branch in the vicinity of the photostimuli, the spatial distribution of responses represents a measure of the spatial resolution. After the experiment, the dendritic arborizations of the recorded neurons were reconstructed. Only cells where the apical dendrite did not ramify within 100 μm of the photostimulation sites were included for analysis. For the light intensities used for sCRACM mapping, the full-width at half-maximum of the spatial profile of the responses was 59 ± 14 μm ($n = 4$; Supplementary Fig. 3b, c). Higher laser intensities degraded the resolution slightly.

To verify this resolution estimate within our data set, we identified stretches of unbranched L5 apical dendrites that received input from ChR2-positive axons originating either in VPM, L4 or L2/3. Only inputs separated from branch points by at least 100 μm were used. In addition, to avoid over-representation of a subset of inputs, we only scored inputs that were at least 100 μm apart. Detectable EPSC$_{sCRACM}$ were only evoked within 75 μm of the apical dendrite (Supplementary Fig. 3d, e). We conclude that sCRACM maps specific types of input with ~60-μm spatial resolution.

Data in the text are given as mean ± s.d.

31. Shepherd, G. M., Pologruto, T. A. & Svoboda, K. Circuit analysis of experience-dependent plasticity in the developing rat barrel cortex. *Neuron* **38**, 277–289 (2003).
32. Williams, S. R. & Stuart, G. J. Site independence of EPSP time course is mediated by dendritic I(h) in neocortical pyramidal neurons. *J. Neurophysiol.* **83**, 3177–3182 (2000).
33. Nevian, T., Larkum, M. E., Polsky, A. & Schiller, J. Properties of basal dendrites of layer 5 pyramidal neurons: a direct patch-clamp recording study. *Nature Neurosci.* **10**, 206–214 (2007).
34. Stepanyants, A., Hof, P. R. & Chklovskii, D. B. Geometry and structural plasticity of synaptic connectivity. *Neuron* **34**, 275–288 (2002).